



# Design and Implementation of Electroceutical for the Treatment of Alzheimer's Disease in Primates

Whi-Young Kim

*Department of Digital Healthcare, Pusan Healthcare University, Busan 49318, Republic of Korea*  
*Corresponding Author: Whi-Young Kim*

Date of Submission: 24-08-2023

Date of Acceptance: 06-09-2023

## ABSTRACT:

Disease infections typically initiate from an inflammatory stage, and initial treatment approaches involve chemical methods to regulate metabolic functions. If these prove inadequate or result in side effects, physical treatment methods become necessary. As these chemical methods are administered through the bloodstream, millions of cases of drug-related side effects occur annually, aside from the intended disease. This limitation prevents the reflection of pathological physiology. Particularly concerning brain disorders and dementia-related cortical responses, plasticity, and connectivity, cautious consideration is crucial. Moreover, in cases of Alzheimer's disease, the initial brain atrophy and the strength of stimulation coil distance are influential factors. The excessive activation of the cortex and the increased volume of cerebrospinal fluid due to brain atrophy alter the characteristics of brain tissue, and induced currents by magnetic stimulation have adverse effects. The stimulation site encroaches on non-motor cortex areas biochemically and metabolically, and changes in the motor cortex area lead to subsequent issues. In this study, we aim to implement a portable medical device based on a micro bio-processor that supports energy-efficient biofeedback stimulation system functions. This device includes neural sensing, stimulation, two stable wireless connections, high-efficiency power management, and wireless charging, tailored for electronic drug applications. To construct a closed-loop system based on neuronal characteristics, a pulse loop is implemented using ion rhodium current (IRh), chronaxie time (TCh), and refractory period (TRefractory), utilizing 180nm HV BCD technology.

**KEYWORDS:** Electroceutical, Treatment, Alzheimer's Disease, Primates

## I. INTRODUCTION

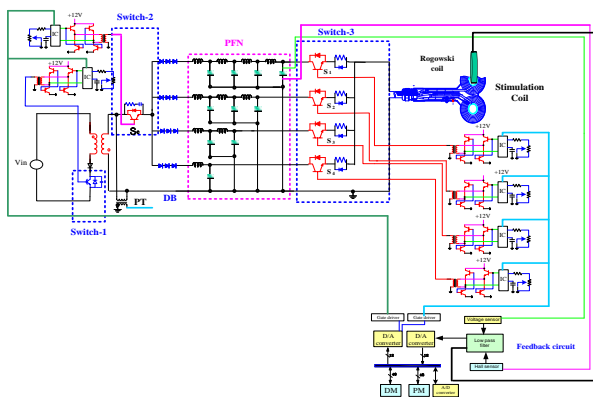
In general, when utilizing brain neurostimulation devices for brain disorders and dementia, these devices primarily stimulate the motor cortex regardless of the state of the brain disorder. This approach fails to reflect the pathophysiology, and careful consideration is necessary for cortical reactivity, plasticity, and connectivity related to brain disorders and dementia-related cortex. Brain atrophy itself is associated with cortical hyperactivity, altering brain tissue characteristics and influencing induced currents due to increased cerebrospinal fluid volume. Issues related to the stimulation site predominantly involve non-motor cortex areas, according to biochemical and metabolic studies on Alzheimer's dementia. Changes in the motor cortex area emerge later[1].

Especially in the context of Alzheimer's disease, the initial brain atrophy and the strength of stimulation coil distance are influential factors. Excessive cortical activation and increased cerebrospinal fluid volume due to brain atrophy have negative impacts on the characteristics of brain tissue and currents induced by magnetic stimulation. The levels of amyloid- $\beta$  and t-Tau proteins in cerebrospinal fluid influence the effectiveness of brain neurostimulation. High levels of t-Tau, as suggested by Koch and others, necessitate enhanced stimulation effects for Alzheimer's dementia patients. Therefore, controlling the levels of amyloid- $\beta$  and t-Tau in cerebrospinal fluid during brain neurostimulation is crucial. The integration of EEG sensors with brain neurostimulation devices holds advantages in distinguishing cortical enhancement and inhibition effects concerning cortical connectivity. A linkage device between brain neurostimulation devices and EEG sensors is required to evaluate physiological changes and connectivity within the brain beyond the motor cortex area. Customized stimulation for brain disorder patients based on the shape of the cerebral cortex, and delivering appropriate therapeutic pulses for altered cerebral cortex forms



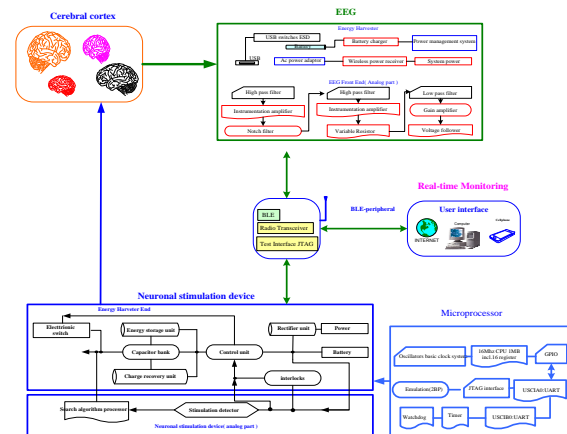
due to lesions, should be implemented using pulse-forming devices. These devices should also allow real-time monitoring via cell phones, computers, and the web, serving various purposes in brain disorder treatment. Particularly, transplantable neural electrical stimulation can be used for epilepsy treatment (Vagus nerve stimulation (VNS)), deep brain stimulation for Parkinson's disease, and functional electrical stimulation (FES) to restore impaired bodily functions. Central nervous system injuries in the CNS lead to various neurological disorders like stroke, depression, epilepsy, and Parkinson's disease, with neural regulation replacing impaired functions[2]. Neural regulation of the peripheral nervous system's Vagus nerve, which connects critical organs like brown adipose tissue, liver, pancreas, to the brain, is relatively facilitated by electronic drug application. In this study, Phase 2 stimulation involves connecting current sinks and sources to the tissue for a specific period. Current pulse parameters such as polarity, pulse width, separation, amplitude, and repetition period vary based on specific applications[3]. Typically, these are composed of pulse profile data and 5-9 bits of current amplitude data. The necessary current amplitude for stimulation in each cycle is provided by the current mode DAC based on this amplitude data. The DAC input is the quantized value of the acquired stimulation signal from the outside, and the PI controller mechanism continuously maintains the analog value[3]. The current in the DAC alternates between current sinks and sources in a continuous manner, mirroring polarity for both cathodic and anodic phases in a typical CMOS stimulation driver[12].

## II. Basic concept of Electroceutical in Medicine for Nerve Cell Treatment



In Figure 1, the algorithm of this study

Figure 1 illustrates the overall approach proposed in this study. Due to process and load variations, a discrepancy of around 2-5% occurs between the current amplitudes of cathodic and anodic phases, leading to charge imbalance within the tissue. For biological safety, a charge balance state, which signifies that the charge accumulation over a certain period is not permitted, needs to be maintained.



In Figure 2, the algorithm of this study is based on the biological characteristics of neurons.

As the typical values are in the order of several hundred nanofarads, on-chip implementation faces challenges. Another effective method is periodic shorting of the electrodes for sufficient time to discharge[4]. In general electronic drug applications, implantable devices consist of subsystems such as power and data, clock, recovery, stimulation data generation, stimulation, and remote sensing devices.

In Figure 2, the algorithm of this study is based on the biological characteristics of neurons. Refractory period refers to the recovery time when excitatory neurons return to their resting state and prepare for the next stimulation. When a neuron is in the TRefractory state, it should not be excited by any stimulation. Applying stimulation current to neurons during TRefractory leads to the wastage of E-STIM. An E-S device with a feedback loop can find the optimal AMP, PW, and FREQ along the SD curve.

$$AMP = TCh, FREQ = 1/TRefractory \quad (1)$$

Once the E-S device identifies the optimal parameters mentioned above, it can apply a stimulation current tailored to the target neuron for



optimal excitation. With the ability to set optimal stimulations, the device can save numerous instances of E-STIM, leading to significant energy conservation. After passing through the second-order high-pass filter, the signal is converted from voltage to current using an adjustable transconductance. The signal current is compared to a depolarization threshold current, TH1, generated by an 8-bit current DAC. The depolarization threshold value is typically set as the  $5\sigma$  value of the signal and the comparator remains inactive during the  $\Phi 1$  period, but the reference current is switched to the repolarization threshold value, TH2. If the signal crosses TH2 within the  $\Phi 2$  period, an action potential is detected[5].

The Strength-Duration (SD) curve is introduced in Figure 3, incorporating the concept of electronic drug application[5]. The quantity of charge, Qth, required to induce neural excitation as a threshold, depends on both the intensity (I) and duration (t), with I also dependent on t, indicating a proportional relationship[6].

$$Q_{th}(I(t), t) = I(t) * t \quad (2)$$

$$I(t) = A * (1 + B/t) \quad (3)$$

When both A and B are constant values:

$A = IR_h$ , and biologically, it signifies the minimum intensity that induces infinite-duration excitation in neurons[7].

$B = TCh$ , and when the intensity is  $2 * IR_h$ , it represents the minimum duration, the point at which the minimum ESTIM triggers neural excitation.

$$= f\left(\frac{1}{n}\right)\frac{1}{n} + f\left(\frac{2}{n}\right)\frac{1}{n} + f\left(\frac{3}{n}\right)\frac{1}{n} + \dots + f\left(\frac{k}{n}\right)\frac{1}{n} + \dots + f\left(\frac{n}{n}\right)\frac{1}{n} \quad (4)$$

$$= \sum_{k=1}^n f\left(\frac{k}{n}\right)\left(\frac{1}{n}\right) \quad (5)$$

$$\sum_{k=0}^{n-1} f\left(\frac{k}{n}\right)\left(\frac{1}{n}\right) = \sum_{k=0}^{n-1} \left(\frac{k}{n}\right)^2 \left(\frac{1}{n}\right) = \sum_{k=1}^{n-1} \frac{k^2}{n^3} = \frac{1}{n^3} \sum_{k=1}^{n-1} k^2 = \frac{1}{n^3} \frac{n(n-1)(2n-1)}{6} \quad (6)$$

$$\lim_{n \rightarrow \infty} S_n = \lim_{n \rightarrow \infty} \frac{n(n+1)(2n+1)}{6n^3} \quad (7)$$

$$= f\left(\frac{0}{n}\right)\frac{1}{n} + f\left(\frac{1}{n}\right)\frac{1}{n} + f\left(\frac{2}{n}\right)\frac{1}{n} + f\left(\frac{k}{n}\right)\frac{1}{n} + f\left(\frac{n-1}{n}\right)\frac{1}{n} \quad (8)$$

$$\sum_{k=0}^{n-1} f\left(\frac{k}{n}\right)\left(\frac{1}{n}\right) \quad (9)$$

$$= \sum_{k=0}^{n-1} f\left(\frac{k}{n}\right)\left(\frac{1}{n}\right) = \sum_{k=0}^{n-1} \left(\frac{k}{n}\right)^2 \left(\frac{1}{n}\right) = \sum_{k=1}^{n-1} \frac{k^2}{n^3} = \frac{1}{n^3} \sum_{k=1}^{n-1} k^2 = \frac{1}{n^3} \frac{n(n-1)(2n-1)}{6} \quad (10)$$

$$= \sum_{k=1}^n f\left(\frac{k}{n}\right)\left(\frac{1}{n}\right) \quad (11)$$

$$= \sum_{k=0}^{n-1} f\left(\frac{k}{n}\right)\left(\frac{1}{n}\right) \quad (12)$$

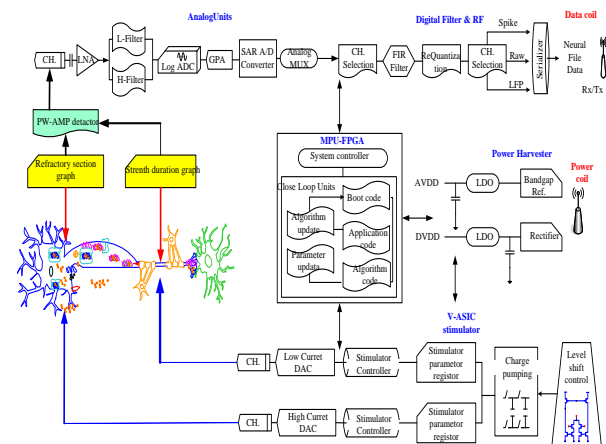


Figure 3 illustrates that the fiber activation threshold depends not only on the stimulation intensity but also on the stimulation duration.

Hence, with stronger stimulation, more fibers reach the threshold. The fiber activation threshold varies not only with stimulation intensity but also with stimulation duration[8].

Depolarization of excitable membranes requires the flow of charge across the membrane. Due to the dominant membrane capacitance, a relevant parameter for effective membrane depolarization is the total charge delivered across the membrane. For a short-duration stimulus generating a constant transmembrane current, the delivered charge (Q) is proportional to the product of current (I) and time (T).

$$Q = I \times T \quad (16)$$

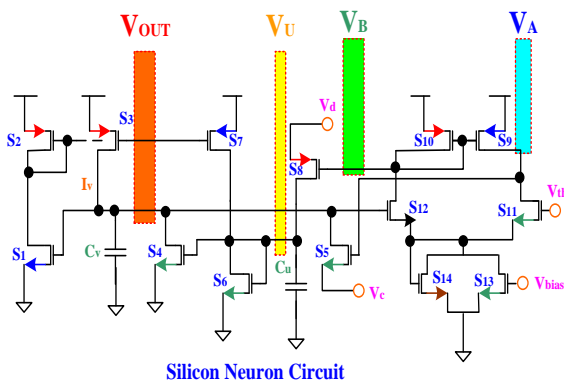
Therefore, the current (It) required to achieve activation, considering the delivered charge (Q t) necessary to activate the fibers and the stimulation duration (D), is given by the following equation.



$$t = Q t / D \text{---(17)}$$

The intensity-duration curve for a typical nerve membrane is similar, but it significantly differs by reaching a flat curve at longer stimulation durations, converging towards a point called the RHEOBASE[9]. In Figure 4, a silicon neural circuit is depicted, and if the actual stimulus strength is below the Rheobase, even with very long stimulation durations, the stimulus remains ineffective. During extended periods of stimulation, the equation fails to predict the charge movement across the neural membrane. If the stimulus is too weak, the membrane potential doesn't reach the threshold[10],[11].

Commonly, the refractory period corresponds to the period associated with the movement of image points on the left branch of the iso-intensity lines. In physiology, it's the period in which a response or a specific action is repeated or impossible.



Silicon Neuron Circuit

In Figure 4, a silicon neural circuit is configured.

Time-dependent excitability in membrane A is prepared by the second stimulus and returns to the refractory state after excitation. This commonly refers to electrically excitable muscle cells or neurons. The absolute refractory period corresponds to depolarization and repolarization, while the relative refractory period corresponds to hyperpolarization. In electrochemistry, after the action potential initiation, the absolute refractory period is defined in two ways: the entire duration of the action potential and the period when Na<sup>+</sup> channels that opened for depolarization of the original membrane become inactivated due to channel inactivation until the membrane is hyperpolarized. The channels remain inactivated until the membrane is over-hyperpolarized, at which point the channels close and become

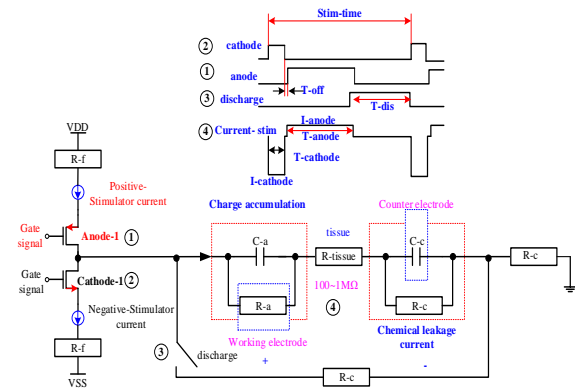
inactive, recovering their ability to respond to stimuli and open.

The relative refractory period immediately follows the absolute period, and similarly, it ends the action potential by repolarizing the voltage-gated potassium channel membrane. This results in a rapid increase in the membrane's potassium conductance. The movement of K<sup>+</sup> ions out of the cell makes the membrane potential closer to the potassium equilibrium potential, causing a transient membrane hyperpolarization, meaning the membrane potential temporarily becomes more negative than the normal resting potential. The neuron's refractory period occurs after the action potential, typically lasting about 1 millisecond. The action potential consists of three phases: depolarization, when voltage-gated sodium ion channels open, increasing the neuron's membrane conductance to sodium ions, and the cell's membrane potential is depolarized. The membrane becomes less negative and when the potential reaches the activation threshold (-55mV), depolarization is actively driven by the neuron and goes beyond the equilibrium potential of the activated membrane (+30mV). Repolarization, the second phase, involves inactivation of the voltage-gated sodium ion channels due to the now depolarized membrane and activation of voltage-gated potassium channels. Both the inactivation of sodium ion channels and the opening of potassium ion channels repolarize the cell's membrane potential back to the resting membrane potential.

### III Proposal of Electrochemical for Nerve Cell Treatment:

#### 3-1. Electrochemical Model

The required nonlinear oscillatory behavior in Figure 5 is achieved by using the differential equations of the two-state variables as described by Izhikevich (2003), along with a separate spike-after-reset mechanism. However, the goal is to use the simplest possible circuitry of analog VLSI implementation that can replicate the functional behavior of the coupled system of nonlinear equations.



In Figure 5, the required nonlinear oscillatory behavior is achieved using the differential equations of the two-state variables as described by Izhikevich (2003), along with a separate spike-after-reset mechanism.

The positive feedback current is generated by S1 and mirrored by S2~S3, with a roughly quadratic dependence on the membrane potential. The magnitude of the current provided by S7 is determined by the membrane potential in a manner similar to membrane circuits. Transistor (S6) provides nonlinear leakage current. Transistors and capacitances are adjusted to make the potential C2 change more slowly than C1. Following the membrane potential spike, a comparator generates a short pulse to turn on transistor S8, allowing additional charge controlled by the voltage of node W5 to be transferred to C2 [12].

This circuit is designed and fabricated using 0.35µm CMOS technology. Because most of the transistors in this circuit operate in strong inversion, the firing pattern is about 10<sup>4</sup> times faster than biological real-time in an "accelerated" time scale. The power consumption of the circuit is less than 10pJ/spike.

A similar circuit has been presented by Wijekoon and Dudek (2009), but it operates in weak inversion and provides spike timing on the biological timescale. Figure 5 is a schematic overview of the Izhikevich neuron circuit, and it's implemented in 0.35µm CMOS VLSI technology.

### 3-2. Electroceutical configuration

Figure 6 is designed to represent the horizontal control approach for the electroceutical method being pursued in this study. Particularly, the initial implementation in electroceuticals needs to consider portable stimulator devices, and several

factors should be addressed during the design. The key stimulation parameters include amplitude, pulse width, and stimulation rate, where the size of the stimulation current should exceed the threshold value leading to the generation of action potentials. The stimulator can provide an output current in the range of 32µA to 1mA, covering various neural stimulation applications. Figure 7 is designed while considering current stimulation and charge balance. The stimulation pulse width of the design is set to 100µs, and the rate is set at 400µs. After the stimulation phase, the active charging balancing phase occurs within a 50µs timing window. In addition to the design parameters, power efficiency and small footprint for multichannel implementation are also required. In this approach, an electrode model with tissue resistance values of RE = 100MΩ, CE = 200nF, and 100kΩ is assumed. To deliver a 1mA current to a load of 10kΩ, a minimum compliance of 10V voltage is required. The proposed stimulator employs standard CMOS transistors at 1.8V and 3.3V for typical operation.

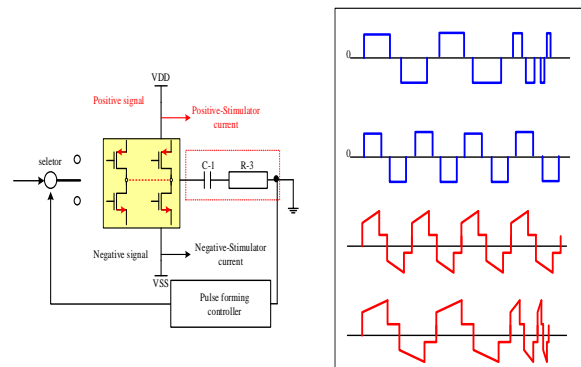


Figure 6 illustrates the design of the electroceutical method that the study aims to establish, employing a horizontal control approach.

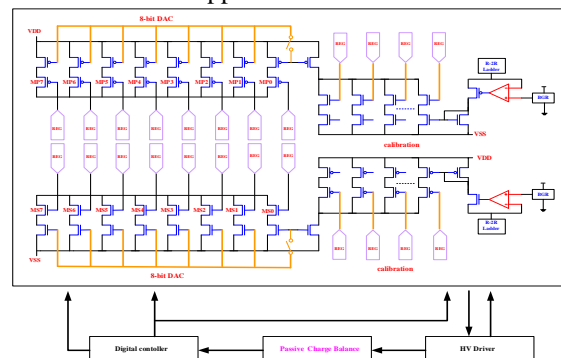


Figure 7 represents the design considering current stimulation and charge balance.



### 3-3. Electrode-electrolyte interface model

To achieve matching amplitudes for the cathodic and anodic current pulses, a self-calibration technique is required. For pulse amplitudes around  $\sim 3\text{mA}$ , the amplitude difference between the two pulses can be reduced to less than  $2\mu\text{A}$  after calibration.

The functionality of the stimulator is to generate stimulation current pulses. Neural signal detection might need to be performed between two consecutive stimulation pulses. Neural signal detection should be executed at the nominal electrode potential, which is the same as the potential before the stimulation pulse is applied. Frequencies in applications are generally below  $100\text{Hz}$ .

The pulse duration is set to the same value within the range of  $20\mu\text{s}$  to several hundred  $\mu\text{s}$ . The amplitude of the cathodic and anodic current pulses ranges from a few hundred  $\mu\text{A}$  to several  $\text{mA}$ , depending on the application.

### 3-4. Charge Balancing

Figure 8 illustrates that neural stimulation is achieved by delivering charge to neural tissue through conductive electrodes. This is accomplished by applying a constant stimulation current over a certain period of time. Electric decomposition is induced, which can lead to electrode dissolution, pH changes, and tissue damage. A straightforward method to prevent charge accumulation is adopting a two-phase stimulation pulse along with the current source. The DC current is maintained at  $I_{dc} < 10\text{nA}$  to prevent the accumulation of charge, which could lead to strong Faraday currents.

On the other hand, the stimulation current is known to be  $1\text{mA}$ . In practical integrated circuits, this can be challenging, thus alternative charge-balancing techniques are proposed. Firstly, the blocking capacitor needs to be significantly larger than the interface capacitor (CE) since it must integrate the total stimulation charge. It also needs to be implemented externally.

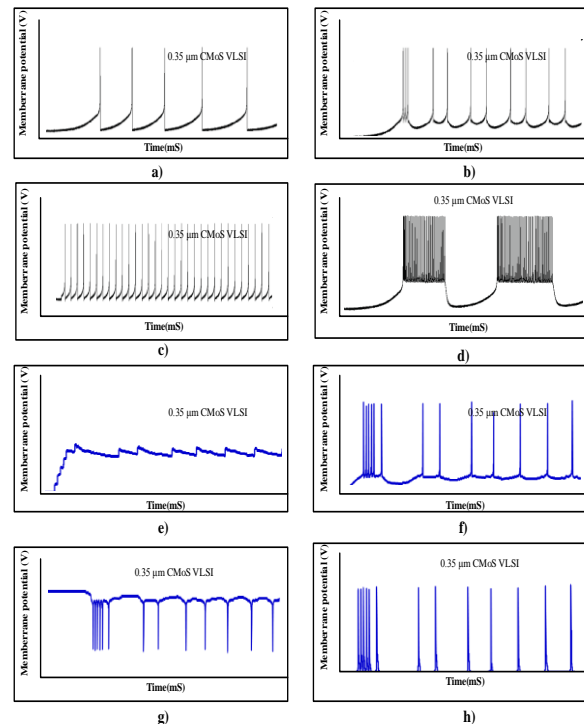


Figure 8 depicts neural stimulation, which involves delivering charge to neural tissue through conductive electrodes.

### 3-5. Current Driver

Feedback control charge balancing technique has been proposed to actively regulate excessive electrode potentials within a safe range. Since only the counter electrode or the stimulating electrode can be electrically connected, direct access to this voltage is not possible. It's possible to measure  $V_{CE} \approx \Delta V_E$  without any current flow.

When  $V_E > V_{CM} \pm \Delta V_E$ , a safe range, after measurements, a small charge packet of the possible polarity is applied using a stimulus current source to neutralize excessive electrode potentials. Verification and charging operations are repeated until the electrode potential falls within the safe window. As a result, the interaction occurs through the counter electrode capacitor. The current is a typical stimulation current, and due to its very short duration, underscores the importance of stability considerations. Replacing the linear mode driver with a switching network can minimize power losses in the electrical stimulator.



### 3-5. DAC

In the 2-phase stimulator design shown in Figure 7, cathodic current pulses and anodic current pulses are generated by NMOS Current Digital-to-Analog Converter (nDAC) and PMOS Current Digital-to-Analog Converter (pDAC), respectively. To prevent tissue damage and electrolysis at the electrodes, the average DC leakage current should be less than 100 – 300nA. Incorporating a low DC leakage capacitor between the stimulator and the electrode is preferred for safety reasons, but it can generate an average mismatch current that charges the capacitor.

As a result, the output voltage of the stimulator can drift close to the supply rail due to this mismatch current. Due to feedback, the parameters AMP, PW, and FREQ are optimized to their minimum values for neural induction. To allocate the power budget, the IREF generator, including BGR, OPAMP, and R-2R calibration network, consumes the most at 9.83uA in the low-voltage domain of VDD.

The CE driver consumes 7.22uA, and the stimulation channel including WE driver, charge balance window, and digital controller consumes 6.3uA each. In the high-voltage domain VDDH, all bias currents, including VREF generator, IREF generator, and HV amplifier, are consumed by the CE driver, totaling 10.6uA. Without applying the proposed technique, AMP, PW, FREQ, and VDDH are 2mA, 2ms, 500Hz, and 9V, respectively. However, with the closed-loop in place, these parameters can be optimized to 0.5mA, 400us, 200Hz, and 3V.

In this approach, the Band Gap Reference (BGR) generates a stable VREF of 600mV, while the OPAMP, along with an R-2R ladder calibration bank, creates a stable IREF of 31.25uA using VREF. IREF, copied into IDAC with an 8-bit code, results in ISTIM\_MAX being 8mA. An additional IDAC with a 4-bit code for calibration, where LSB is (1/16) \* IREF, is present. The Working Electrode (WE) driver applies the stimulation current to the target neuron, supplied by a high-voltage source, compliance voltage, and VDDH. For ensuring linearity and simplifying control circuitry, a cascade current steering architecture is chosen over other DAC architectures. The designed DAC generates currents from 4 to 128uA in 4uA steps, thus minimizing current consumption. This current is amplified eightfold in the output driver stage.

### 3-6. Current Mirror OTA-Based Driver

The discrepancies within the output driver circuit in Figure 7 lead to variations in current amplitude during each phase of stimulation. While these discrepancies might not be critical for a single stimulation cycle, they can accumulate residual charges after each stimulation cycle. Excessive voltage differences can potentially damage the tissue, so it's essential to keep them below 100mV. To compare the two electrodes, both are directly connected to a low-voltage comparator. During one clock cycle, the comparator assesses the voltage difference between the two electrodes. In the charge balance phase, the comparator consists of multiple low-voltage operational transconductance amplifiers (OTAs), and the total current consumption is less than 2uA. The input-referred noise spectrum density of this OTA is given by (8.6), where gm1 represents the transconductance of the input devices M1, M5, M6, and M7.

$$v_1^2(f) = \frac{16}{3_1} \left( 1 + 2 \frac{g_1}{g_1} + \frac{g_1}{g_1} \right) \text{-----}(18)$$

gm3 represents the transconductance of the nMOS current mirror devices M21-M3, while gm7 characterizes the transconductance of the pMOS current mirror devices M1, M8, and M11, M12. To minimize the input-referred noise of the OTA, you ensure that gm1 >> gm3, gm7. This is achieved by adjusting the sizes of transistors M4, M6, M5, and M7 to operate in a region where the ratio of transistor transconductance is weakly inverted. The drain current (gm/ID) is at its maximum, and M21 to M11 operate deeply in a strong inversion where gm/ID decreases significantly.

The dimensionless performance metric that captures the essence of this trade-off is the proposed Noise Efficiency Factor (NEF). NEF helps assess the noise performance considering the power consumption and gain characteristics of the amplifier. It gives insight into how efficiently the noise is amplified compared to the power consumed by the circuit.

$$NEF = V_1 \sqrt{\frac{2I_t}{\pi \cdot U_T \cdot 4kT \cdot BW}} \text{-----}(19)$$

The total amplifier supply current, denoted as I\_total, relates to the thermal voltage kT/q, where k is Boltzmann's constant, T is absolute temperature, and q is the elementary charge. BW represents the amplifier bandwidth, and Vni,rms stands for the amplifier's input-referred RMS voltage noise. An



amplifier with noise generated solely by the thermal noise of an ideal bipolar transistor results in  $NEF = 1$ . For all physical circuits,  $NEF > 1$ . In modern IC amplifiers, while the supply voltage only varies by about 5 times, the supply current can vary by orders of magnitude (e.g., from 1nA to 1A). As a result, NEF is closely related to power consumption.

NEF is a metric used to assess the efficiency of noise amplification compared to the power consumed by the circuit. It provides valuable insights into how well an amplifier is able to balance noise performance and power efficiency in practical designs.

#### IV. Implementation Result

Figure 8 illustrates the parameter optimizer's procedure, which first seeks to find the optimal amplitude. By varying the amplitude between its minimum and maximum settings, the optimizer identifies the optimal amplitude. When the experimental PW is set to 2.50ms (instead of infinity), the resulting error in achieving the ideal IRh remains under 10%. However, if no response is detected in the spike detector, the optimizer incrementally increases the amplitude in steps of 2.50ms. The reason behind linearly adjusting the amplitude is to prevent the neuron from jumping into the refractory state (TRefractory).

The subsequent step involves finding the optimal PW. This process is quite similar to finding the optimal amplitude, but the initial AMP is set to 2 times IRh. In this step, the PW is initially set to a minimum of 2.50ms, and it's linearly increased to avoid entering the TRefractory state. During these traction steps, the optimizer can identify the stimulus that consumes the least energy for a single pulse (AMP \* PW).

The final step is determining the optimal inter-pulse duration (FREQ). The optimizer sets AMP and PW to their optimal values and begins with FREQ at its maximum value, which corresponds to the shortest inter-pulse duration. While the ES device delivers stimulating current to the target neuron, the spike detector monitors neural responses and calculates whether each pulse can induce a response. In Figure 9, the end of the TRefractory state signifies the occurrence of another neural stimulus, and any pulses during this period are disregarded.

Since middle three stimulation pulses didn't induce responses, the optimizer can determine the optimal FREQ to be  $1/TRefractory$ . In active charge balancing, the active charge

balancer hasn't been extensively researched in the past. This voltage isn't directly accessible as only the relative electrode or stimulating electrode can be electrically connected. As long as there's a flow of current, this voltage mainly exhibits a significant "resistive" voltage drop across tissue impedance, rather than the voltage across the interface capacitance. Measurement of  $VCE \approx \Delta VE$  can be performed without current flow.

While precise values might not be crucial, excessive voltage only becomes important if it exceeds the safe voltage window around the common-mode potential. In Figure 9, when neural stimulation occurs again, it marks the end of the TRefractory state, and any pulses during this period..

If  $VE > VCM \pm \Delta VE$ , a safe condition is met. To address excessive electrode voltages, a small charge packet of the possible polarity is applied using a stimulation current source after measurement. This can be achieved through current spikes or other implementations. As a result, the proposed technique is introduced in feedback-controlled charge-balancing technology, actively adjusting excessive electrode potentials within the safety window. This provides precise control over safe operating conditions for both the system and operators. Stability must be considered in a feedback system. It's important that various stimulation sites can counteract each other. The charge balancer bases its operation on comparing the electrode's voltage VE with the reference electrode's VCM. Consequently, it also shows a voltage on the electrode's capacitor voltage VCE, and additionally on the voltage of the large electrode VCCE.

Figure 10 depicts a micrograph of the biofeedback stimulator chip. The proposed IC is fabricated using a 180nm HV BCD process and occupies a chip area of 2mm x 2.3mm. The performance of the stimulator is summarized in the table. It dissipates biases of 23.4uA and 10.6uA in the VDD and VDDH domains, respectively. Stimulation parameters can be programmed within the range of 31.25uA-8mA, 10us-2.55ms, and DC-1kHz. The proposed IC is fabricated using a 180nm HV BCD process and occupies a chip area of 1.5mm x 1.5mm. The stimulator's performance is summarized in the table. It can program complex waveforms within the range of 31.25uA-8mA, 10us-2.55ms, DC-1kHz, 255 pulses/train/cluster, and a maximum duration of 24 hours. It can emulate four types of neural spikes based on the mathematical Izhikevich SNC model. In Figure 10, the first two cases demonstrate appropriate balance,



with the controller's time constant (4.7ms) being greater than the stimulation period (2ms). The controller has lower gain and smaller time constants than the stimulation period. The balancing current in this case is similar to pulse insertion techniques but with very small balancing charge per cycle.

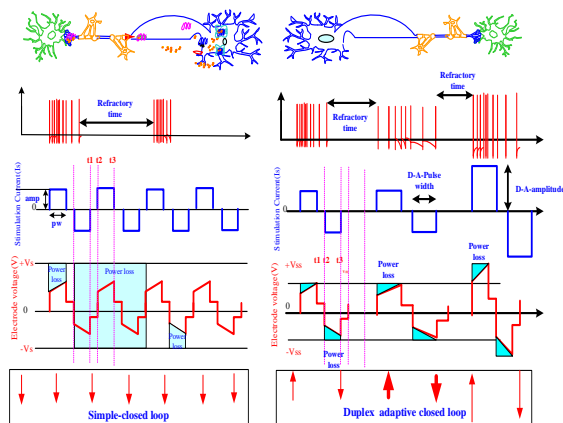


Figure 9 shows a microscopic image of the biofeedback stimulator chip.

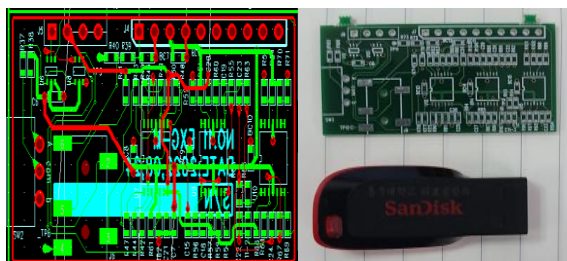


Figure 10 represents a product board implemented with the actual electronic medicine concept.

Finally, when the offset balancing current is controlled at a high level, with substantial gain and a large time constant, the electrode's resting potential can shift over time between positive and negative threshold values. Whenever the electrode potential drops below 100mV, the offset balancer significantly increases the balancing current to step up the resting potential to a higher value. These outcomes align with the effects of very small time constants, too large or too small offset current updates, and the impact on the resting potential. Decreasing AMP, PW, FREQ, and VDH, which respectively denote amplitude, pulse width, stimulation current frequency, and supply voltage of the current driver, is crucial for enhancing the lifespan of ES devices, usually accounting for more

than 99% of the total energy consumption, and these devices are supplied with limited-lifespan batteries. In this approach, a closed loop can be formed to adjust stimulation current from the closed-loop, thereby extending the lifespan of ES devices. Figure 11 depicts a product board implemented with the actual electronic medicine concept.

In the case of conventional devices, they can only provide electrical stimulation to the target neuron and cannot read the target state before and after stimulation. After several iterations of the closed-loop process involving stimulation, detection, and adjustment, the device can find the optimal parameters that induce the same response in the target neuron, exceeding its neural threshold value. The recovery time signifies the period when excitatory neurons return to their dormant state, allowing them to prepare for the next stimulation. During the T-Refractory state, neurons should not be excited by any stimulation. Measurement results before and after applying the closed-loop to the device are shown. When the proposed technique is not applied, AMP, PW, FREQ, and VDDH were 2.1mA, 2.1ms, 500Hz, and 9.2V, respectively. By applying the closed-loop to the system, the parameters can be optimized to 0.6mA, 404us, 200Hz, and 3.1V.

## V. Conclusion

Electroceutical is being actively researched not only for challenging chronic diseases like dementia, Alzheimer's, rheumatoid arthritis, colitis, and asthma, but also for complex and incurable conditions such as cancer, Parkinson's disease, and more. As successful cases of electronic medicine emerge, there is a growing interest in developing advanced forms of electronic medicine that could replace traditional pharmaceuticals. Global IT companies are increasingly focusing on these developments, and as a result, the related market is expected to expand. CMOS-based neural stimulation systems are extensively developed for various implantable biomedical applications, including neural prosthetics to restore limb movements, implants aiding visual recovery in visually impaired patients, and more. They are also used for deep brain stimulation (DBS) purposes in epilepsy patients. The fundamental concept of neural stimulation involves controlled delivery of controlled positive charges to initiate actions and recovery, stimulating degenerated or damaged neurons within the brain or the body.



In this study, a high-quality programmable neural mimicking stimulator IC was developed, capable of generating numerous pulses, trains, and clusters with dead-time slots, extending the duration of a single therapy up to 24 hours. A new stimulation method based on the SNC artificial neuron model was proposed and implemented to mimic the behavior of neuron cells. The proposed stimulator IC driven by the SNC model can output four types of neural spikes with a power consumption of 10uW.

For long-lifespan portable medical applications, there's a need for energy-efficient biofeedback stimulation systems, and the development aims to extend their lifespans. To achieve this, novel device reduction techniques such as adaptive parameter optimization and closed-loop algorithms based on the biological characteristics of neurons are employed. The electronic medicine configuration through algorithms successfully found optimal stimulation parameters, including AMP, PW, FREQ, and VDDH.

#### Acknowledgements

“It was supported as an industry-academia joint technology development project of the 2023 LINC3.0 project.”

#### References

- [1]. E. Wassermann, Oxford handbook of Transcranial Stimulation, Oxford University Press, Oxford (2007).
- [2]. C. Edward Coffey and Jeffrey L. Cummings, The American Psychiatric Publishing Textbook of Geriatric Neuropsychiatry, American Psychiatric Press (2011).
- [3]. M. Sommer, N. Lang, F. Tergau, and W. Paulus, Neuroreport 13, 809 (2002).
- [4]. S.-S. Choi, Journal of Biomedicine and Biotechnology 278062 (2011).
- [5]. R. S. J. Frackowiak, K. J. Friston, and C. Frith, Human brain function, 2nd ed., Academic Press, San Diego, (2003).
- [6]. Nicole A. Lazar, The Statistical Analysis of Functional MRI Data. Springer, Berlin (2008).
- [7]. Orrin Devinsky and Aleksandar Beric, Electrical and magnetic stimulation of the brain and spinal cord, Raven Press, New York (1993).
- [8]. Richard S. J. Frackowiak, John T. Ashburner, William D. Penny, Semir Zeki, Karl J. Friston, Christopher D. Frith, Raymond J. Dolan, and Cathy J. Price, Human Brain Function, Second Edition (2004).
- [9]. S. S. Choi, J. Magn. 15, 210 (2010).
- [10]. Mark S. George and Robert H. Belmaker, Transcranial Magnetic Stimulation in Clinical Psychiatry (2006).
- [11]. Walter J. Levy, Roger Q., M. D. Cracco, Anthony T. Barker, and J. C. Rothwell, Magnetic Motor Stimulation: Basic Principles and Clinical Experience (1991).
- [12]. M. Inghilleri, A. Berardelli, P. Marchetti, and M. Manfredi, Exp. Brain. Res. 109, 467 (1996).